

Orbital Hall effect in mesoscopic devices

Diego B. Fonseca,¹ Lucas L. A. Pereira,¹ and Anderson L. R. Barbosa^{1,*}

¹Departamento de Física, Universidade Federal Rural de Pernambuco, 52171-900, Recife, PE, Brazil

(Dated: May 3, 2023)

We investigate the orbital Hall effect through a disordered mesoscopic device with momentum-space orbital texture that is connected to four semi-infinite terminals embedded in the Landauer-Büttiker configuration for quantum transport. We present clear analytical and numerical evidence that the orbital Hall current fluctuations are universals (as with spin Hall current fluctuations). The universal orbital Hall current fluctuations (UOCF) exhibit two universal numbers of 0.36 and 0.18 for weak and strong spin-orbit coupling, respectively. The universal numbers are obtained by analytical calculation via random matrix theory and are supported by numerical calculations based on the tight-binding model. Furthermore, the UOCF lead to two universal relationships between the orbital Hall angle and conductivity. Finally, we confront the two universal relations with experimental data of the orbital Hall angle, which shows good concordance between theory and experiment.

PACS numbers:

Introduction - The Spin Hall effect (SHE) is one of the most prominent phenomena observed in spintronics, which allows us to convert a longitudinal charge current to a transversal spin Hall current (SHC) [1–9]. Spin-orbit coupling (SOC) is the key behind the SHE because it lets us control spin transport properties without magnetic materials. Furthermore, the spin Hall angle (SHA) is an important parameter that is commonly used to quantify a material’s ability to convert charge-to-spin currents. SHA is defined as the ratio between the SHC and the charge current, and has been measured in various heavy metals—that is, metals with strong SOC, such as Pt [10], and W [11]—and in two-dimensional materials—such as graphene [12, 13].

Much attention has been given to the orbital Hall effect (OHE), which is a phenomenon of orbitronics [14–42]. As shown by D. Go *et.al.* [17], we can convert a longitudinal charge current to a transversal orbital Hall current (OHC) in centrosymmetric systems with momentum-space orbital texture, even when the orbital angular momentum is quenched in equilibrium. A remarkable feature of OHE is that it is independent of SOC, in contrast with SHE. Therefore, we can consider the OHE to be more fundamental than the SHE [17, 25]. Similar to SHA, the orbital Hall angle (OHA) quantifies a material’s ability to convert charge-to-orbital currents and was measured in light metals as Ti [34, 35] and Cr [36] (i.e., metals with weak SOC) and heavy metals as W [35] and Pt [36].

As shown in the 1980s [43], the charge current through the disordered mesoscopic device in the linear regime at low temperature exhibits universal mesoscopic fluctuations, which are theoretically interpreted within the framework of random matrix theory (RMT) [44]. Therefore, in the early SHE experiments [3, 4], the interest in whether the SHC exhibits universal fluctuations appeared. The universality of SHC fluctuations was numer-

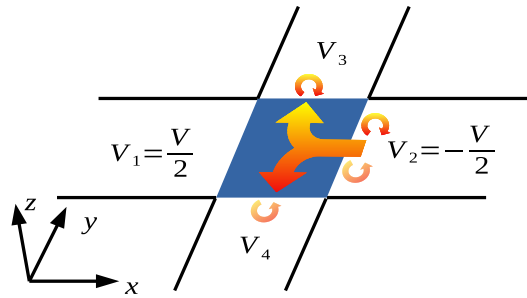


FIG. 1: OHE through a disordered mesoscopic device with space-moment orbital texture (blue) connected to four semi-infinite terminals subjected to voltages V_i . The SOC may or may not be included in the mesoscopic device.

ically demonstrated by [45] and confirmed analytically via RMT [46]. However, the universal SHC fluctuations (USCF) have never been confirmed experimentally because the SHC is only measured indirectly via the inverse spin Hall effect [47–50]. The connection between USCF and SHE experiments was made by [51, 52], who show that the USCF lead to a universal relationship between the maximum SHA deviation Θ_{SH} and dimensionless longitudinal conductivity $\sigma = Nl_e/L$, where N , L and l_e are the number of propagating wave modes, longitudinal device length, and free electron path, respectively, which is given by $\Theta_{\text{SH}} \times \sigma = 0.18$. Therefore, the question that arises in the early OHE experiments is [33–36]: does the OHC exhibit universal fluctuations?

In this Letter, we study the OHE through a disordered mesoscopic device with momentum-space orbital texture that is connected to four semi-infinite terminals that are embedded in the Landauer-Büttiker configuration for quantum transport, as shown in Fig.(1). Using analytical calculations via RMT and numerical calculations based on the tight-binding model for a square lattice with four orbitals, we report the universality of OHC fluc-

tuations with different universal numbers for light and heavy metals. Furthermore, the universal OHC fluctuations (UOCF) lead to two universal relationships between the maximum OHA deviation and dimensionless longitudinal conductivity. Finally, we confront the two universal relations with experiment data of [34–36], and conclude the compatibility between theory and experiments.

Orbital Hall effect - We designed the OHE setup through a mesoscopic device with orbital angular momentum and spin degrees of freedom that is connected to four semi-infinite terminals that are submitted to voltages V_i , Fig.(1). From the Landauer-Büttiker model, the OHC (SHC) through the i th terminal in the linear regime at low temperature is

$$I_{i,\eta}^{o(s)} = \frac{e^2}{h} \sum_j \tau_{ij,\eta}^{o(s)} (V_i - V_j), \quad (1)$$

where the orbital (spin) transmission coefficient is calculated from the transmission and reflection blocks of scattering matrix $\mathcal{S} = [\mathcal{S}_{ij}]_{i,j=1,\dots,4}$

$$\tau_{ij,\eta}^{o(s)} = \text{Tr} \left[(\mathcal{S}_{ij})^\dagger \mathcal{P}_\eta^{o(s)} \mathcal{S}_{ij} \right].$$

The matrix $\mathcal{P}_\eta^{o(s)} = \mathbb{1}_N \otimes l^\eta \otimes \sigma^0 (\mathbb{1}_N \otimes l^0 \otimes \sigma^\eta)$ is a projector, where $\mathbb{1}_N$ is a identity matrix with dimension $N \times N$. The dimensionless integer N is the number of propagating wave modes in the terminals, proportional to the terminal width (W) and the Fermi vector (k_F) through the equation $N = k_F W / \pi$. The index $\eta = \{0, x, y, z\}$, $l^0 = (l^\eta)^2$, $\sigma^0 = (\sigma^\eta)^2$, and l^η and σ^η are orbital angular momentum and Pauli matrices, respectively. Therefore, the charge current is defined by $\eta = 0$, while OHC (SHC) by $\eta = \{x, y, z\}$.

The pure OHC (SHC) $I_{i,z}^{o(s)} = I_i^{o(\uparrow)} - I_i^{o(\downarrow)}$, $i = 3, 4$ can be obtained by assuming that the charge current vanishes in the transverse terminals, $I_{i,0}^c = I_i^{o(\uparrow)} + I_i^{o(\downarrow)} = 0$, while the charge current is conserved in the longitudinal terminals, $I_{1,0}^c = -I_{2,0}^c = I^c$ [5, 46, 53]. By applying these conditions to Eq.(1), we obtain [54]

$$I_{i,\eta}^{o(s)} = \frac{e^2}{h} \left[\left(\tau_{i2,\eta}^{o(s)} - \tau_{i1,\eta}^{o(s)} \right) \frac{V}{2} - \tau_{i3,\eta}^{o(s)} V_3 + \tau_{i4,\eta}^{o(s)} V_4 \right], \quad (2)$$

for $i = 3, 4$, where V is a constant potential difference between longitudinal terminals, and $V_{3,4}$ is the transversal terminal voltage. The nature of the OHC is a charge current moving through the orbital degrees of freedom projected by \mathcal{P}_η^o .

We consider a mesoscopic device with disorder Fig.(1), which allows us to analyse the OHE in the framework of RMT [44]. Without an external magnetic field applied, the mesoscopic device preserves time-reversal symmetry. Therefore, the scattering matrix is described by the circular orthogonal ensemble (COE) when SOC is

absent (light metals) and the circular symplectic ensemble (CSE) when SOC is strong (heavy metals). Consequently, we can calculate the average and variance of the OHC (2) by applying the method of [55]. The calculation is valid for the ballistic chaotic and diffusive mesoscopic devices in the limit when the mean dwell time of the electrons is much longer than the time needed for ergodic exploration of the phase space, $\tau_{\text{dwell}} \gg \tau_{\text{erg}}$ [44].

Without loss of generality, we consider a mesoscopic device with four orbitals (i.e., s and p orbitals) and $\eta = z$. In this case

$$l^z = \begin{bmatrix} 0 & 0 & 0 & 0 \\ 0 & 0 & -i & 0 \\ 0 & i & 0 & 0 \\ 0 & 0 & 0 & 0 \end{bmatrix}, \quad \sigma^z = \begin{bmatrix} 1 & 0 \\ 0 & -1 \end{bmatrix},$$

and the scattering matrix has dimension $32N \times 32N$. To perform the average of Eq.(2), we must take the experimental regime of interest; that is, when the sample has a large thickness $N \gg 1$. Therefore, we can assume the central limit theorem (CLT) [56] and expand Eq.(2) in the function of N [44]. By applying the method of [55] in Eq.(2), we find

$$\langle I_\eta^{o(s)} \rangle = 0, \quad (3)$$

for COE and CSE. The SHC average was previously calculated by [46, 57, 58]. Eq.(3) implies a zero-mean Gaussian distribution, meaning all relevant information can be contained in OHC fluctuations. Therefore, we are interested in the OHC deviation because although the mean of one is zero, its fluctuations can be significant.

In the usual way, we define the OHC deviation as

$$\text{rms}[I_\eta^o] = \sqrt{\langle I_\eta^{o2} \rangle - \langle I_\eta^o \rangle^2} = \sqrt{\langle I_\eta^{o2} \rangle},$$

and by applying the method of [55], we obtain [54]

$$\text{rms}[I_\eta^o] = \frac{e^2 V}{h} \times \begin{cases} \sqrt{\frac{1}{8}} & \text{approx. 0.36 for COE} \\ \sqrt{\frac{1}{32}} & \text{approx. 0.18 for CSE} \end{cases}, \quad (4)$$

for $\eta = \{x, y, z\}$. Meanwhile, $\text{rms}[I_\eta^s] = 0$ and 0.18 for COE and CSE, respectively [46, 57, 58]. Eq.(4) is the first outcome of this work, which indicates that the OHC fluctuations are universal, as with SHC fluctuations [45]. UOCF of light metals (COE) are consistent with the interpretation that the OHE is more fundamental than the SHE because it is independent of SOC. Furthermore, when the SOC is increased, the UOCF of light metals (COE) is decreased by a factor of 2 to UOCF of heavy metals (CSE) because SOC breaks the spin-rotation symmetry. In this case, UOCF and USCF exhibit the same universal number.

Orbital Hall angle - Motivated by recent experiments of OHA [34–36] and by the fact that the OHC fluctuations

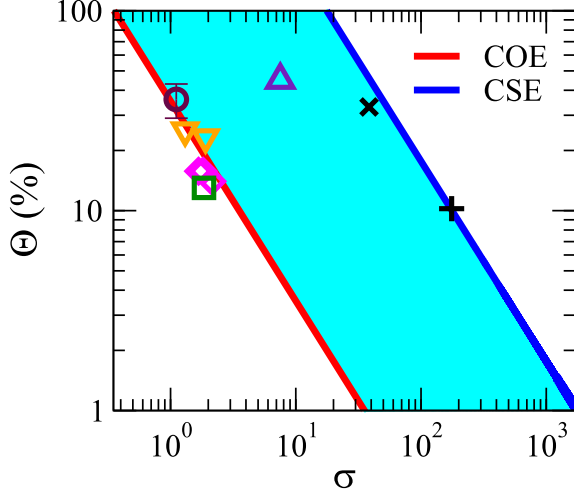


FIG. 2: The figure shows the $\Theta_{\text{OH}}(\%)$ and $\Theta_{\text{SH}}(\%)$ as a function of dimensionless conductivity σ . The circle symbol is experimental data of OHA for Ti [34]. The square and triangle up symbols are experimental data of OHA for Ti and W [35], respectively. The triangles down and diamonds symbols are experimental data of $\Theta_{\text{LS}}(\%)$ for Cr and Pt [36], respectively. The plus and times symbols are experimental data of SHA for Pt [10] and W [11], respectively. The lines are the Eq.(10).

are unassailable experimentally, we use Eq.(4) to obtain two universal relations that characterize the OHA. The OHA is defined as the ratio between OHC and charge current

$$\Theta_{\text{OH}} = \frac{I^o}{I^c}. \quad (5)$$

To compute the average of Eq.(5), we assume the experimental regime $N \gg 1$. Therefore, we have to resort to the CLT and expand (5) in the function of N [51, 52]. The average of (5) can be approximated by

$$\langle \Theta_{\text{OH}} \rangle = \left\langle \frac{I^o}{I^c} \right\rangle \approx \frac{\langle I^o \rangle}{\langle I^c \rangle}. \quad (6)$$

By substituting Eq.(3) in Eq.(6), we conclude that

$$\langle \Theta_{\text{OH}} \rangle = 0, \quad (7)$$

for COE and CSE. An equivalent result was obtained for SHA [51, 52], $\langle \Theta_{\text{SH}} \rangle = 0$. Although the average of OHA is null, there is an expectation that the OHA has large fluctuations because of its direct dependence on the OHC. By following the same methodology that was applied to (4) and (6), we can show that

$$\text{rms}[\Theta_{\text{OH}}] = \frac{\text{rms}[I^o]}{\langle I^c \rangle}. \quad (8)$$

From Eq.(8), we can infer the OHA deviation with the knowledge the OHC deviation and the charge current

average. The former is given by Eq.(4), while the latter is appropriately described by the relation [44, 59]

$$\langle I^c \rangle = \frac{e^2 V}{h} \sigma, \quad (9)$$

where σ is the longitudinal dimensionless conductivity, $\sigma = Nl_e/L$ with $L \gg l_e$. By substituting Eqs.(4) and (9) in (8), we can infer that the maximum OHA deviation is given by

$$\Theta_{\text{OH}} \times \sigma = \begin{cases} 0.36 & \text{for COE} \\ 0.18 & \text{for CSE} \end{cases}. \quad (10)$$

Eq.(10) is the second main outcome of this work. This shows that the product between maximum OHA deviation Θ_{OH} and longitudinal dimensionless conductivity σ holds two universal relationships, which only depend on if the mesoscopic device is a light metal (COE) or a heavy metal (CSE), in contrast with the maximum SHA deviation that holds one relation for heavy metal $\Theta_{\text{SH}} \times \sigma = 0.18$ [51, 52].

Comparison with experiments - To confirm the validity of Eq.(10), we compare it with the recent experimental results of [34–36].

Figure (2) shows $\Theta_{\text{OH}}(\%)$ as a function of σ , where the σ axis is conveniently normalised as $\sigma = \sigma_{\text{exp}}(\Omega^{-1} \cdot \text{cm}^{-1})/10^4(\Omega^{-1} \cdot \text{cm}^{-1})$. The lines are the universal relations for COE and CSE of (10). The cyan area is the *crossover region* (intermediate SOC) between COE (weak SOC) to CSE (strong SOC). The circular symbol is experimental data of OHA from [34], which measured the OHE in a light metal Ti. The light metal has weak SOC, and therefore follows the COE universal relation. The square and triangle up symbols are experimental data of OHA for a light metal Ti and a heavy metal W, respectively, from [35]. Light metal Ti follows the COE, while heavy metal W crossover from COE to CSE. The triangles down and diamonds symbols of Fig.(2) are experimental data of spin-orbital Hall angle $\Theta_{\text{LS}}(\%)$ from [36] for light metal Cr and heavy metal Pt, respectively. They follow the COE universal relation, which is expected to be valid for light metals and indicates a pure OHE [60]. Furthermore, the plus and times symbols are experimental data of $\Theta_{\text{SH}}(\%)$ for heavy metals Pt [10], and W [11], respectively, which follows the CSE [51, 52].

Numerical results - We developed a numerical calculation of OHC (SHC) fluctuations to confirm Eq.(4), and consequently Eq.(10). We use a two-dimensional square lattice device with a momentum-space orbital texture designed as shown in Fig.(1), in which the nearest-neighbor tight-binding model [17, 27] models the lattice with four orbitals (i.e., the s and p orbitals) on each atom. The Hamiltonian is given by [25]

$$H = \left(\sum_{\langle i,j \rangle \alpha \beta \sigma} t_{i\alpha, j\beta} c_{i\alpha\sigma}^\dagger c_{j\beta\sigma} + \text{H.c.} \right)$$

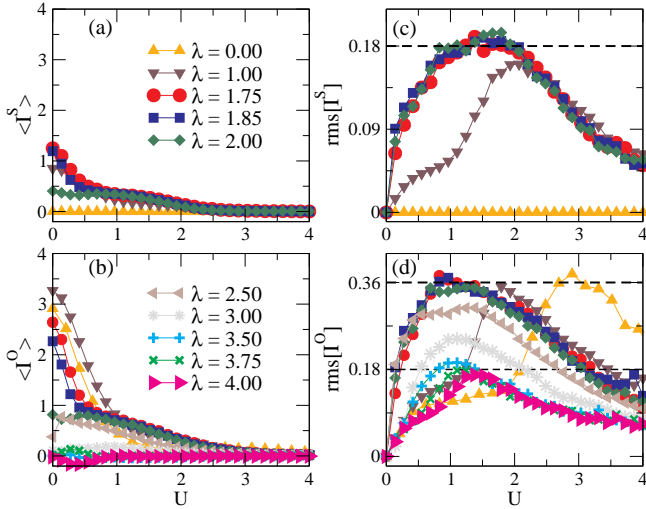


FIG. 3: (a) The SHC and (b) OHC averages (in e^2V/h) as a function of disorder strength U with different SOC strength λ for fixing Fermi energy $E = 2.15$. (c) The SHC and (d) OHC deviations as a function of U . The dashed lines are Eq.(4).

$$+ \sum_{i\alpha\sigma} (E_{i\alpha\sigma} + \epsilon_{i\alpha\sigma}) c_{i\alpha\sigma}^\dagger c_{i\alpha\sigma} \\ + \lambda \sum_{i\alpha\beta\sigma\delta} \sum_{\gamma} c_{i\alpha\sigma}^\dagger L_{\alpha\beta}^\gamma S_{\sigma\delta}^\gamma c_{i\beta\delta}, \quad (11)$$

where $\{i, j\}$, $\{\alpha, \beta\}$, and $\{\sigma, \delta\}$ are the unit cell, orbital, and spin indices, respectively, and $\gamma = \{x, y, z\}$ [54]. The first term represents the nearest-neighbor interaction, where $c_{i\alpha\sigma}$ ($c_{i\alpha\sigma}^\dagger$) is the annihilation (creation) operators and $t_{i\alpha,j\beta}$ denotes hopping integrals. The second is the on-site energy $E_{i\alpha\sigma}$ and Anderson disorder term $\epsilon_{i\alpha\sigma}$. The disorder is realized by an electrostatic potential ϵ_i , which varies randomly from site to site according to a uniform distribution in the interval $(-U, U)$, where U is the disorder strength. The last is the SOC, where λ is the SOC strength, \vec{L} is the angular momentum and \vec{S} is the spin-1/2 operator for the electron. We take the typical Hamiltonian parameters (in eV) $E_s = 3.2$, $E_{px} = E_{py} = E_{pz} = -0.5$ for on-site energies, $t_s = 0.5$, $t_{p\sigma} = 0.5$, $t_{p\pi} = 0.2$, $t_{sp} = 0.5$ for nearest-neighbor hopping amplitudes [17, 27]. The numerical calculations were implemented in the KWANT software [61].

We start by analyzing the SHC fluctuations from Eq.(2) with $\eta = z$ [62]. Figure (3.a) shows the SHC average $\langle I^s \rangle$ (in e^2V/h) as a function of disorder strength U for a fixed Fermi energy $E = 2.15$ and different values of SOC strength λ . As expected, for $\lambda = 0$, the SHC average is always null; while for $\lambda > 0$, it is maximum for $U = 0$ and decreases with increases of U . The SHC deviation is shown in Fig.(3.c) as a function of U . The maximum SHC deviation increases with increases of λ until it reaches the universal number of 0.18, thus becoming independent of λ [45].

We can analyze the OHC fluctuations using Eq.(2) [62].

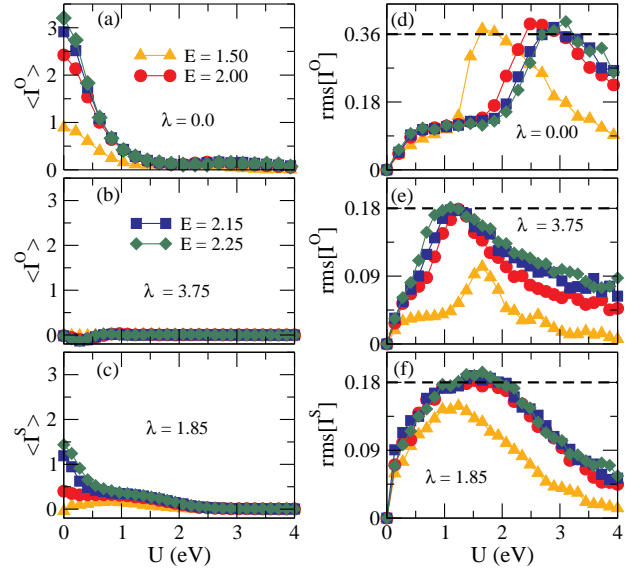


FIG. 4: The OHC average (in e^2V/h) as a function of disorder strength U with fixed SOC strength (a) $\lambda = 0.0$ and (b) $\lambda = 3.75$, and (c) SHC average (in e^3V/h) with $\lambda = 1.85$ for different Fermi energy. Figures (d), (e), and (f) are their respective deviations as a function of U . The dashed lines are Eq.(4).

Figure (3.b) shows the OHC average $\langle I^o \rangle$ (in e^2V/h) as a function of U for $E = 2.15$ and different values of λ . When $\lambda = 0$, the one is maximum for $U = 0$ and decreases with increases of U , in contrast with SHC average Fig.(3.a). Furthermore, the OHC average decreases with increases of λ , in agreement with [17]. The OHC deviation is shown in Fig.(3.d) as a function of U . When $\lambda = 0$, the maximum OHC deviation reaches the universal number of 0.36, which confirms Eq.(4) for light metals (COE). When we increase the SOC strength λ , the maximum OHC deviation remains 0.36. Only for strong SOC does the maximum OHC deviation crossover to the universal number of 0.18, thus confirming Eq.(4) for heavy metals (CSE). This behavior explains why the experimental data of W is on the *crossover region* of Fig.(2). The latter indicates that the SHE and OHE happen together, and their quantitative contributions cannot be disentangled [36]. This also is consistent with the interpretation that the OHC is efficiently converted to SHC [33] because the SHC does not need a strong SOC to reach 0.18, see Fig.(3.c).

To confirm the robustness of our results, we fixed the SOC strength and changed the Fermi energy. Figures (4.a) and (4.b) show the OHC average as a function of U for $\lambda = 0$ and $\lambda = 3.75$, respectively, while Fig.(4.c) shows the SHC average with $\lambda = 1.85$ for different values of Fermi energy. Their respective deviations are shown in Figs.(4.d), (4.e), and (4.f). For light metal $\lambda = 0$ (4.d), the maximum OHC deviation reaches a universal number of 0.36 (COE) independent of Fermi energy. In contrast,

for heavy metal $\lambda = 3.75$ (4.d), the one reaches the universal number of 0.18 (CSE), which confirms that OHC fluctuations are universals with universal numbers given by Eq.(4). Finally, Fig.(4.f) shows that the maximum SHC deviation reaches 0.18 [45].

Conclusions - We have demonstrated the universality of OHC fluctuations. The UOCF displays two universal numbers of 0.36 and 0.18 for light (COE) and heavy (CSE) metals (4), respectively; in contrast to the USCF, which displays a universal number of 0.18 for heavy metals (CSE). The UOCF leads to two universal relationships between the maximum OHA deviation and the dimensionless conductivity σ given by (10). The two universal relationships are in agreement with the experimental data of [34–36], Fig.(2). The results are calculated analytically via RMT and supported by numerical calculations based on the tight-binding model. This work brings a new perspective on OHE and may help to give a deeper understanding of the effect. Furthermore, similar to what happens with USCF [52, 58, 63], we expect that UOCF in topological insulators [21, 22] follow the same universal values of (4) when $N \gg 1$. The presented methodology can be extended to other effects, such as the spin Nernst effect [64], giving rise to a set of universal relationships, such as (10).

DBF acknowledges a scholarship from Fundação de Amparo a Ciência e Tecnologia de Pernambuco (FACEPE, Grant IBPG-0253-1.04/22). ALRB acknowledges financial support from Conselho Nacional de Desenvolvimento Científico e Tecnológico (CNPq, Grant 309457/2021).

* Electronic address: anderson.barbosa@ufrpe.br

- [1] M. Dyakonov and V. Perel, Physics Letters A **A 35**, 459 (1971), URL [https://doi.org/10.1016/0375-9601\(71\)90196-4](https://doi.org/10.1016/0375-9601(71)90196-4).
- [2] J. E. Hirsch, Phys. Rev. Lett. **83**, 1834 (1999), URL <https://link.aps.org/doi/10.1103/PhysRevLett.83.1834>.
- [3] Y. K. Kato, R. C. Myers, A. C. Gossard, and D. D. Awschalom, Science **306**, 1910 (2004), ISSN 0036-8075, URL <https://science.scienmag.org/content/306/5703/1910>.
- [4] J. Wunderlich, B. Kaestner, J. Sinova, and T. Jungwirth, Phys. Rev. Lett. **94**, 047204 (2005), URL <https://link.aps.org/doi/10.1103/PhysRevLett.94.047204>.
- [5] B. K. Nikolić, L. P. Zárbo, and S. Souma, Phys. Rev. B **72**, 075361 (2005), URL <https://link.aps.org/doi/10.1103/PhysRevB.72.075361>.
- [6] R. Raimondi, C. Gorini, P. Schwab, and M. Dzierzawa, Phys. Rev. B **74**, 035340 (2006), URL <https://link.aps.org/doi/10.1103/PhysRevB.74.035340>.
- [7] C. Gorini, in *Reference Module in Materials Science and Materials Engineering* (Elsevier, 2022), ISBN 978-0-12-803581-8, URL <https://www.sciencedirect.com/science/article/pii/B9780323908009001013>.
- [8] J. Sinova, S. O. Valenzuela, J. Wunderlich, C. H. Back, and T. Jungwirth, Rev. Mod. Phys. **87**, 1213 (2015), URL <https://link.aps.org/doi/10.1103/RevModPhys.87.1213>.
- [9] A. Avsar, H. Ochoa, F. Guinea, B. Özyilmaz, B. J. van Wees, and I. J. Vera-Marun, Rev. Mod. Phys. **92**, 021003 (2020), URL <https://link.aps.org/doi/10.1103/RevModPhys.92.021003>.
- [10] E. Sagasta, Y. Omori, M. Isasa, M. Gradhand, L. E. Hueso, Y. Niimi, Y. Otani, and F. Casanova, Phys. Rev. B **94**, 060412 (2016), URL <https://link.aps.org/doi/10.1103/PhysRevB.94.060412>.
- [11] C.-F. Pai, L. Liu, Y. Li, H. W. Tseng, D. C. Ralph, and R. A. Buhrman, Applied Physics Letters **101**, 122404 (2012), <https://doi.org/10.1063/1.4753947>, URL <https://doi.org/10.1063/1.4753947>.
- [12] J. Balakrishnan, G. Kok Wai Koon, M. Jaiswal, A. H. Castro Neto, and B. Özyilmaz, Nature Physics **9**, 284 (2013), URL <https://doi.org/10.1038/nphys2576>.
- [13] J. Balakrishnan, G. K. W. Koon, A. Avsar, Y. Ho, J. H. Lee, M. Jaiswal, S.-J. Baeck, J.-H. Ahn, A. Ferreira, M. A. Cazalilla, et al., Nature Communications **102**, 4748 (2014), URL <https://doi.org/10.1038/ncomms5748>.
- [14] B. A. Bernevig, T. L. Hughes, and S.-C. Zhang, Phys. Rev. Lett. **95**, 066601 (2005), URL <https://link.aps.org/doi/10.1103/PhysRevLett.95.066601>.
- [15] T. Tanaka, H. Kontani, M. Naito, T. Naito, D. S. Hirashima, K. Yamada, and J. Inoue, Phys. Rev. B **77**, 165117 (2008), URL <https://link.aps.org/doi/10.1103/PhysRevB.77.165117>.
- [16] V. o. T. Phong, Z. Addison, S. Ahn, H. Min, R. Agarwal, and E. J. Mele, Phys. Rev. Lett. **123**, 236403 (2019), URL <https://link.aps.org/doi/10.1103/PhysRevLett.123.236403>.
- [17] D. Go, D. Jo, C. Kim, and H.-W. Lee, Phys. Rev. Lett. **121**, 086602 (2018), URL <https://link.aps.org/doi/10.1103/PhysRevLett.121.086602>.
- [18] D. Jo, D. Go, and H.-W. Lee, Phys. Rev. B **98**, 214405 (2018), URL <https://link.aps.org/doi/10.1103/PhysRevB.98.214405>.
- [19] L. Salemi, M. Beritta, and P. M. Oppeneer, Phys. Rev. Materials **5**, 074407 (2021), URL <https://link.aps.org/doi/10.1103/PhysRevMaterials.5.074407>.
- [20] L. M. Canonico, T. P. Cysne, A. Molina-Sánchez, R. B. Muniz, and T. G. Rappoport, Phys. Rev. B **101**, 161409 (2020), URL <https://link.aps.org/doi/10.1103/PhysRevB.101.161409>.
- [21] L. M. Canonico, T. P. Cysne, T. G. Rappoport, and R. B. Muniz, Phys. Rev. B **101**, 075429 (2020), URL <https://link.aps.org/doi/10.1103/PhysRevB.101.075429>.
- [22] S. Bhowal and S. Satpathy, Phys. Rev. B **102**, 035409 (2020), URL <https://link.aps.org/doi/10.1103/PhysRevB.102.035409>.
- [23] T. P. Cysne, M. Costa, L. M. Canonico, M. B. Nardelli, R. B. Muniz, and T. G. Rappoport, Phys. Rev. Lett. **126**, 056601 (2021), URL <https://link.aps.org/doi/10.1103/PhysRevLett.126.056601>.
- [24] M. Costa, B. Focassio, L. M. Canonico, T. P. Cysne, G. R. Schleider, R. B. Muniz, A. Fazzio, and T. G. Rappoport, Phys. Rev. Lett. **130**, 116204 (2023), URL <https://link.aps.org/doi/10.1103/PhysRevLett.130.116204>.
- [25] P. Sahu, S. Bhowal, and S. Satpathy, Phys. Rev. B

103, 085113 (2021), URL <https://link.aps.org/doi/10.1103/PhysRevB.103.085113>.

[26] S. Bhowal and G. Vignale, Phys. Rev. B **103**, 195309 (2021), URL <https://link.aps.org/doi/10.1103/PhysRevB.103.195309>.

[27] D. Go and H.-W. Lee, Phys. Rev. Research **2**, 013177 (2020), URL <https://link.aps.org/doi/10.1103/PhysRevResearch.2.013177>.

[28] S. Ding, Z. Liang, D. Go, C. Yun, M. Xue, Z. Liu, S. Becker, W. Yang, H. Du, C. Wang, et al., Phys. Rev. Lett. **128**, 067201 (2022), URL <https://link.aps.org/doi/10.1103/PhysRevLett.128.067201>.

[29] L. Liao, F. Xue, L. Han, J. Kim, R. Zhang, L. Li, J. Liu, X. Kou, C. Song, F. Pan, et al., Phys. Rev. B **105**, 104434 (2022), URL <https://link.aps.org/doi/10.1103/PhysRevB.105.104434>.

[30] S. Ding, A. Ross, D. Go, L. Baldrati, Z. Ren, F. Freimuth, S. Becker, F. Kammerbauer, J. Yang, G. Jakob, et al., Phys. Rev. Lett. **125**, 177201 (2020), URL <https://link.aps.org/doi/10.1103/PhysRevLett.125.177201>.

[31] J. Salvador-Sánchez, L. M. Canonico, A. Pérez-Rodríguez, T. P. Cysne, Y. Baba, V. Clericò, M. Vila, D. Vaquero, J. A. Delgado-Notario, J. M. Caridad, et al., *Generation and control of non-local chiral currents in graphene superlattices by orbital hall effect* (2022), 2206.04565, URL <https://doi.org/10.48550/arXiv.2206.04565>.

[32] S. Han, H.-W. Lee, and K.-W. Kim, Phys. Rev. Lett. **128**, 176601 (2022), URL <https://link.aps.org/doi/10.1103/PhysRevLett.128.176601>.

[33] S. Lee, M.-G. Kang, D. Go, D. Kim, J.-H. Kang, T. Lee, G.-H. Lee, J. Kang, N. J. Lee, Y. Mokrousov, et al., Communications Physics **4**, 234 (2021), URL <https://doi.org/10.1038/s42005-021-00737-7>.

[34] Y.-G. Choi, D. Jo, K.-H. Ko, D. Go, K.-H. Kim, H. G. Park, C. Kim, B.-C. Min, G.-M. Choi, and H.-W. Lee, *Observation of the orbital hall effect in a light metal ti* (2021), URL <https://arxiv.org/abs/2109.14847>.

[35] H. Hayashi, D. Jo, D. Go, T. Gao, S. Haku, Y. Mokrousov, H.-W. Lee, and K. Ando, Communications Physics **6** (2023), URL <https://doi.org/10.1038/2Fs42005-023-01139-7>.

[36] G. Sala and P. Gambardella, Phys. Rev. Res. **4**, 033037 (2022), URL <https://link.aps.org/doi/10.1103/PhysRevResearch.4.033037>.

[37] A. Bose, F. Kammerbauer, D. Go, Y. Mokrousov, G. Jakob, and M. Kläui, *Detection of long-range orbital-hall torques* (2022), URL <https://arxiv.org/abs/2210.02283>.

[38] E. Santos, J. Abrão, D. Go, L. de Assis, Y. Mokrousov, J. Mendes, and A. Azevedo, Phys. Rev. Appl. **19**, 014069 (2023), URL <https://link.aps.org/doi/10.1103/PhysRevApplied.19.014069>.

[39] I. Baek and H.-W. Lee, Phys. Rev. B **104**, 245204 (2021), URL <https://link.aps.org/doi/10.1103/PhysRevB.104.245204>.

[40] A. Bose, F. Kammerbauer, R. Gupta, D. Go, Y. Mokrousov, G. Jakob, and M. Kläui, Phys. Rev. B **107**, 134423 (2023), URL <https://link.aps.org/doi/10.1103/PhysRevB.107.134423>.

[41] D. Go, D. Jo, H.-W. Lee, M. Kläui, and Y. Mokrousov, Europhysics Letters **135**, 37001 (2021), URL <https://dx.doi.org/10.1209/0295-5075/ac2653>.

[42] J. Kim and Y. Otani, Journal of Magnetism and Magnetic Materials **563**, 169974 (2022), ISSN 0304-8853, URL <https://www.sciencedirect.com/science/article/pii/S0304885322008599>.

[43] S. Washburn and R. A. Webb, Advances in Physics **35**, 375 (1986), URL <https://doi.org/10.1080/00018738600101921>.

[44] C. W. J. Beenakker, Rev. Mod. Phys. **69**, 731 (1997), URL <https://link.aps.org/doi/10.1103/RevModPhys.69.731>.

[45] W. Ren, Z. Qiao, J. Wang, Q. Sun, and H. Guo, Phys. Rev. Lett. **97**, 066603 (2006), URL <https://link.aps.org/doi/10.1103/PhysRevLett.97.066603>.

[46] J. H. Bardarson, i. d. I. Adagideli, and P. Jacquod, Phys. Rev. Lett. **98**, 196601 (2007), URL <https://link.aps.org/doi/10.1103/PhysRevLett.98.196601>.

[47] E. Saitoh, M. Ueda, H. Miyajima, and G. Tatara, Applied Physics Letters **88**, 182509 (2006), URL <https://doi.org/10.1063/1.2199473>.

[48] A. Azevedo, L. H. Vilela Leão, R. L. Rodriguez-Suarez, A. B. Oliveira, and S. M. Rezende, Journal of Applied Physics **97**, 10C715 (2005), URL <https://doi.org/10.1063/1.1855251>.

[49] J. B. S. Mendes, O. Alves Santos, L. M. Meireles, R. G. Lacerda, L. H. Vilela-Leão, F. L. A. Machado, R. L. Rodríguez-Suárez, A. Azevedo, and S. M. Rezende, Phys. Rev. Lett. **115**, 226601 (2015), URL <https://link.aps.org/doi/10.1103/PhysRevLett.115.226601>.

[50] J. G. G. S. Ramos, T. C. Vasconcelos, and A. L. R. Barbosa, Journal of Applied Physics **123**, 034304 (2018), URL <https://doi.org/10.1063/1.5010973>.

[51] F. A. F. Santana, J. M. da Silva, T. C. Vasconcelos, J. G. G. S. Ramos, and A. L. R. Barbosa, Phys. Rev. B **102**, 041107 (2020), URL <https://link.aps.org/doi/10.1103/PhysRevB.102.041107>.

[52] J. M. da Silva, F. A. F. Santana, J. G. G. S. Ramos, and A. L. R. Barbosa, Journal of Applied Physics **132**, 183901 (2022), URL <https://doi.org/10.1063/5.0107212>.

[53] B. K. Nikolić and L. P. Zárbo, Europhysics Letters **77**, 47004 (2007), URL <https://dx.doi.org/10.1209/0295-5075/77/47004>.

[54] See Supplemental Material at [URL will be inserted by publisher] for detailed deduction of Eqs. (2) and (4). Numerical confirmation of Eq. (4) through an independent numerical simulation from the random matrix theory model [65, 66]. More details about the tight-binding model Eq. (11).

[55] P. W. Brouwer and C. W. J. Beenakker, Journal of Mathematical Physics **37**, 4904 (1996), URL <https://doi.org/10.1063/1.531667>.

[56] L. E. Reichl, *A modern course in statistical physics* (Arnold, London, 1980), URL <https://cds.cern.ch/record/101976>.

[57] J. G. G. S. Ramos, A. L. R. Barbosa, D. Bazeia, M. S. Hussein, and C. H. Lewenkopf, Phys. Rev. B **86**, 235112 (2012), URL <https://link.aps.org/doi/10.1103/PhysRevB.86.235112>.

[58] T. C. Vasconcelos, J. G. G. S. Ramos, and A. L. R. Barbosa, Phys. Rev. B **93**, 115120 (2016), URL <https://link.aps.org/doi/10.1103/PhysRevB.93.115120>.

//link.aps.org/doi/10.1103/PhysRevB.93.115120.

[59] P. A. Mello and N. Kumar, *Quantum Transport in Mesoscopic Systems* (Oxford, New York, 2004).

[60] The experimental data of conductivity ($\sigma = 1/\rho$) and spin-orbital Hall angle (Θ_{LS}) were taken from Fig. 9 of Ref. [36] for Cr (samples Cr(9)/Tb(3)/Co(2) and Cr(9)/Gd(3)/Co(2)) and Pt (samples Pt(5)/Co, Pt(5)/Co(2)/Gd(4), and Pt(5)/Co(2)/Tb(4)).

[61] C. W. Groth, M. Wimmer, A. R. Akhmerov, and X. Waintal, *New Journal of Physics* **16**, 063065 (2014).

[62] The mesoscopic device has a width and length equal $W = L = 40a$, where a is the square lattice constant. We used 2000 disorder realization to calculate the average and deviation of OHC and SHC shown in Figs. (3) and (4). The numerical results of Figs. (3) and (4) are equivalent for $\eta = \{x, y\}$.

[63] Z. Qiao, J. Wang, Y. Wei, and H. Guo, *Phys. Rev. Lett.* **101**, 016804 (2008), URL <https://link.aps.org/doi/10.1103/PhysRevLett.101.016804>.

[64] S. Meyer, Y.-T. Chen, S. Wimmer, M. Althammer, T. Wimmer, R. Schlitz, S. Geprägs, H. Huebl, D. Ködderitzsch, H. Ebert, et al., *Nature Materials* **16**, 977 (2017), URL <https://doi.org/10.1038/nmat4964>.

[65] J. Verbaarschot, H. Weidenmüller, and M. Zirnbauer, *Physics Reports* **129**, 367 (1985), ISSN 0370-1573, URL <https://www.sciencedirect.com/science/article/pii/0370157385900705>.

[66] F. A. G. Almeida, S. Rodríguez-Pérez, and A. M. S. Macêdo, *Phys. Rev. B* **80**, 125320 (2009), URL <https://link.aps.org/doi/10.1103/PhysRevB.80.125320>.